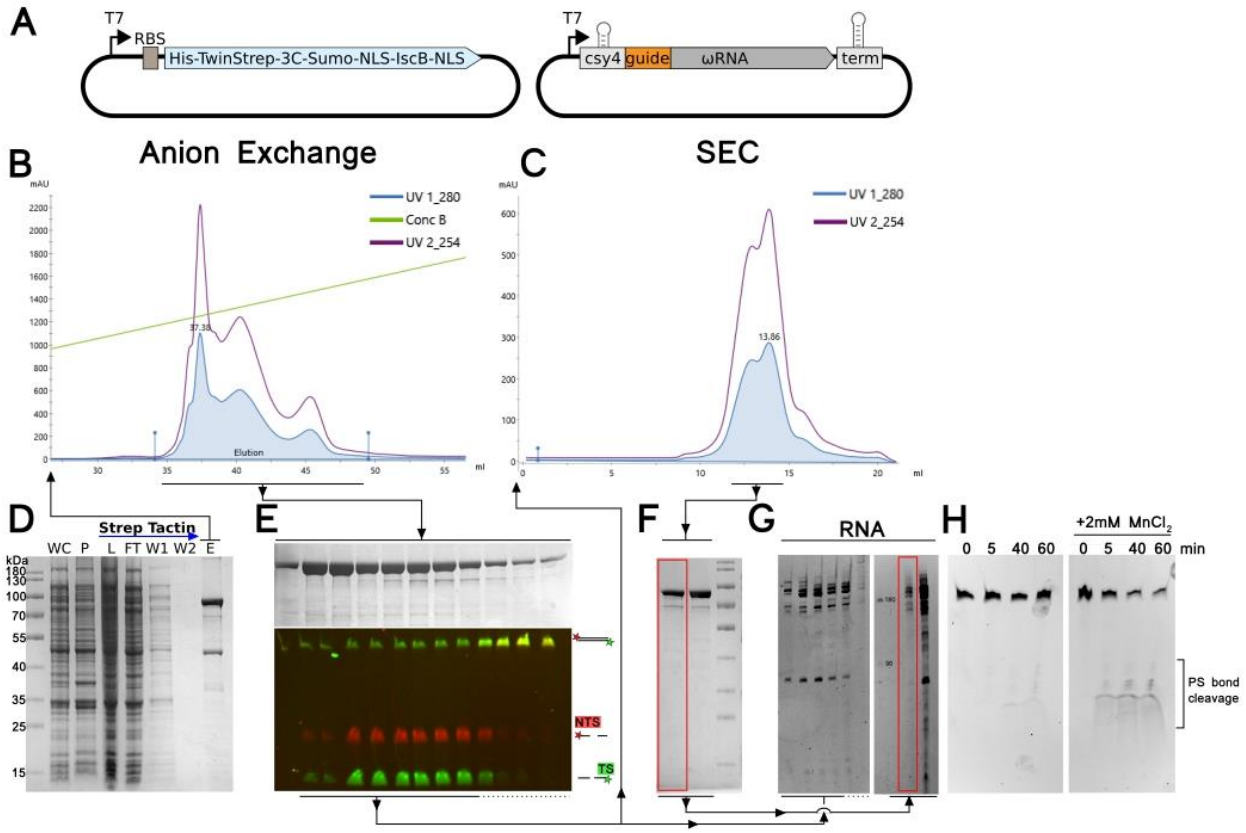

Fig. S1. Reconstitution of the IscB-ωRNA RNP.

(**A**) IscB and ωRNA co-expression scheme. (**B**) Elution profile of the IscB-ωRNA RNP on anion exchange chromatography. (**C**) Elution profile of IscB-ωRNA RNP on size-exclusion chromatography (SEC). (**D**) SDS-PAGE analysis of the Strep-tactin purified IscB-ωRNA RNP. Whole cell (WC), lysed pellet (P), lysate supernatant (L), strep resin flow thru (FT), Dnase I wash (W1), wash2 (W2), elution (E). (**E**) Top: SDS-PAGE of anion exchange peak fractions. Bottom: denaturing-PAGE showing cleavage activity of each fraction. Red channel shows non target strand (NTS). Green channel shows target stand (TS). (**F**) SDS-PAGE of SEC peak fractions. (**G**) Denaturing-PAGE showing the ωRNA quality extracted from IscB RNP. Arrows depict the procedural flow of the purification process. Red boxes depict the final purified sample in SDS-PAGE gel (protein) and Denaturing-PAGE (RNA). (**H**) Denaturing urea-PAGE gel showing time-resolved cleavage reaction of cryo-EM sample NTS-DNA containing phosphorothioate bonds. Minimal cleavage of phosphorothioate bonds observed in standard cleavage conditions. The addition of 2mM $MnCl_2$ is shown to rescue cleavage of NTS-DNA by RuvC.

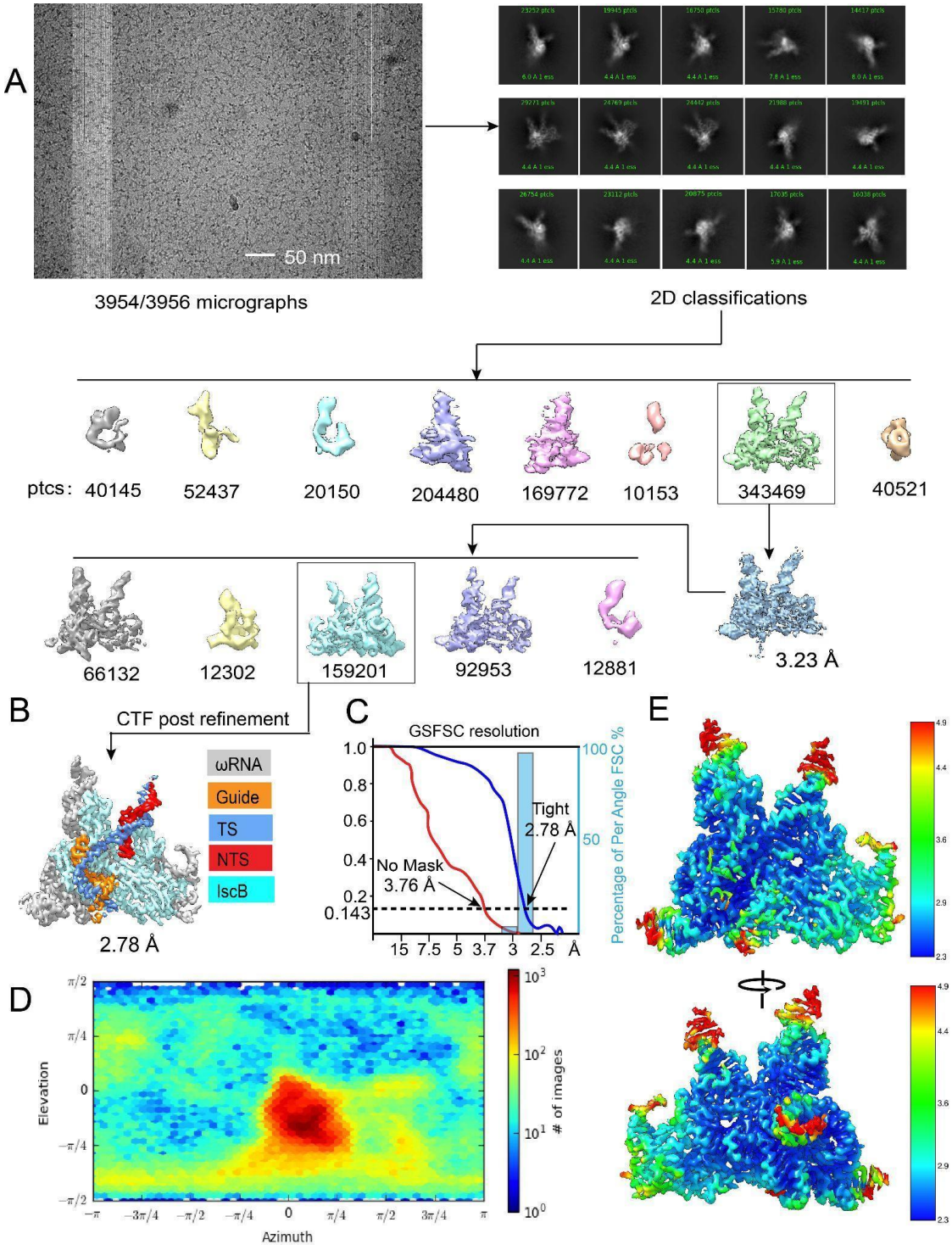

Fig. S2. CryoEM single particle reconstruction of IscB-ωRNA-DNA complex.
(**A**, **B**) Workflow of the cryo-EM image processing and 3D reconstruction for the IscB-ωRNA/DNA complex. Final electron density map with the density from each chain colored separately. **(C**) Fourier Shell Correlations (FSC) of IscB-ωRNA/DNA complex reconstruction, with the gold-standard cutoff (FSC = 0.143) marked with a dotted line. **(D**) Direction distribution plot. (**E**) Final electron density map showing local resolution.

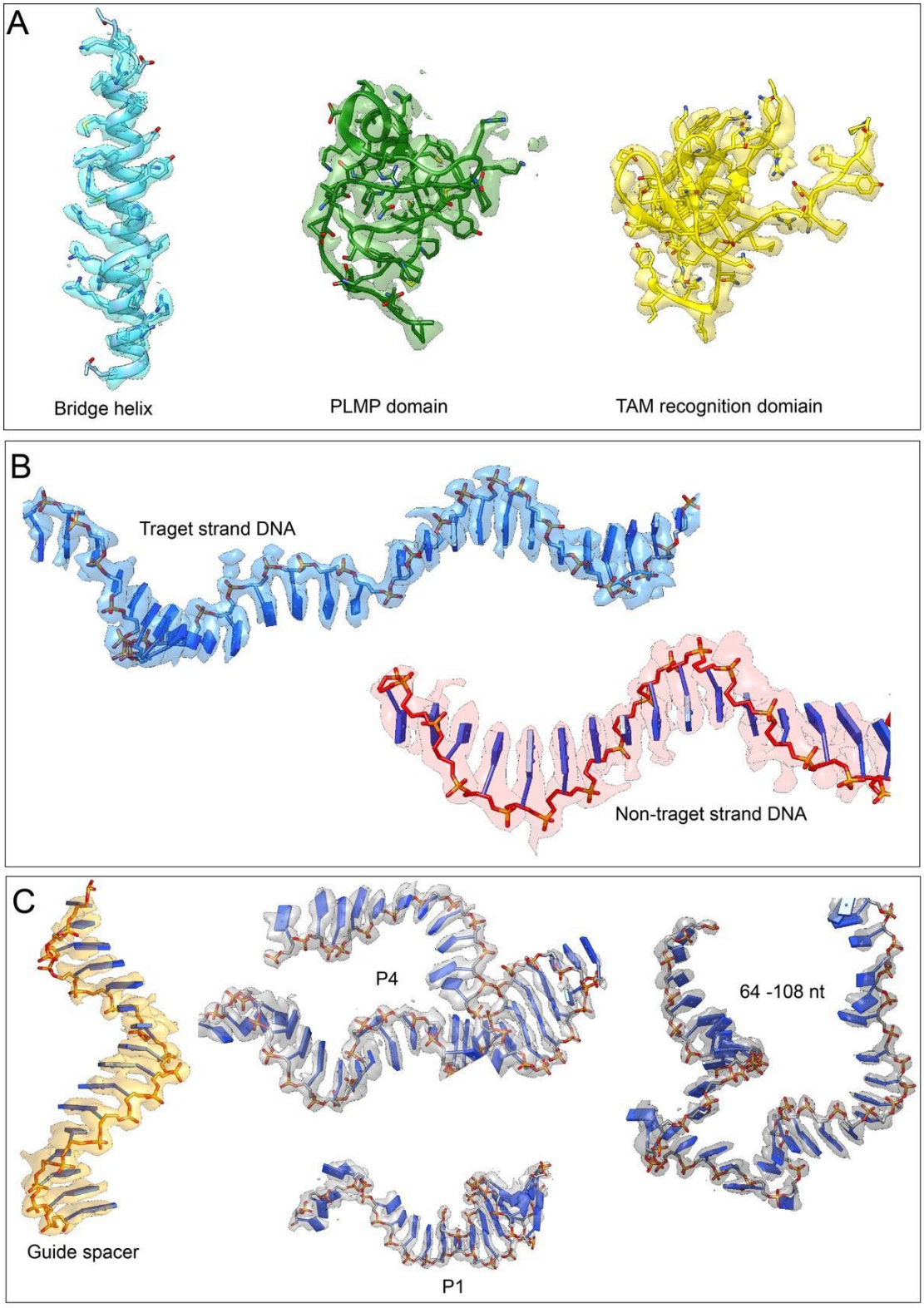

Fig. S3. Representative local map density for the different functional states. **(A)** EM densities for representative protein regions inside IscB-ωRNA/DNA complex. **(B)** EM densities for the target and non-target DNA strands inside the IscB-ωRNA/DNA complex. **(C)** EM densities for representative RNA regions inside IscB-ωRNA/DNA.

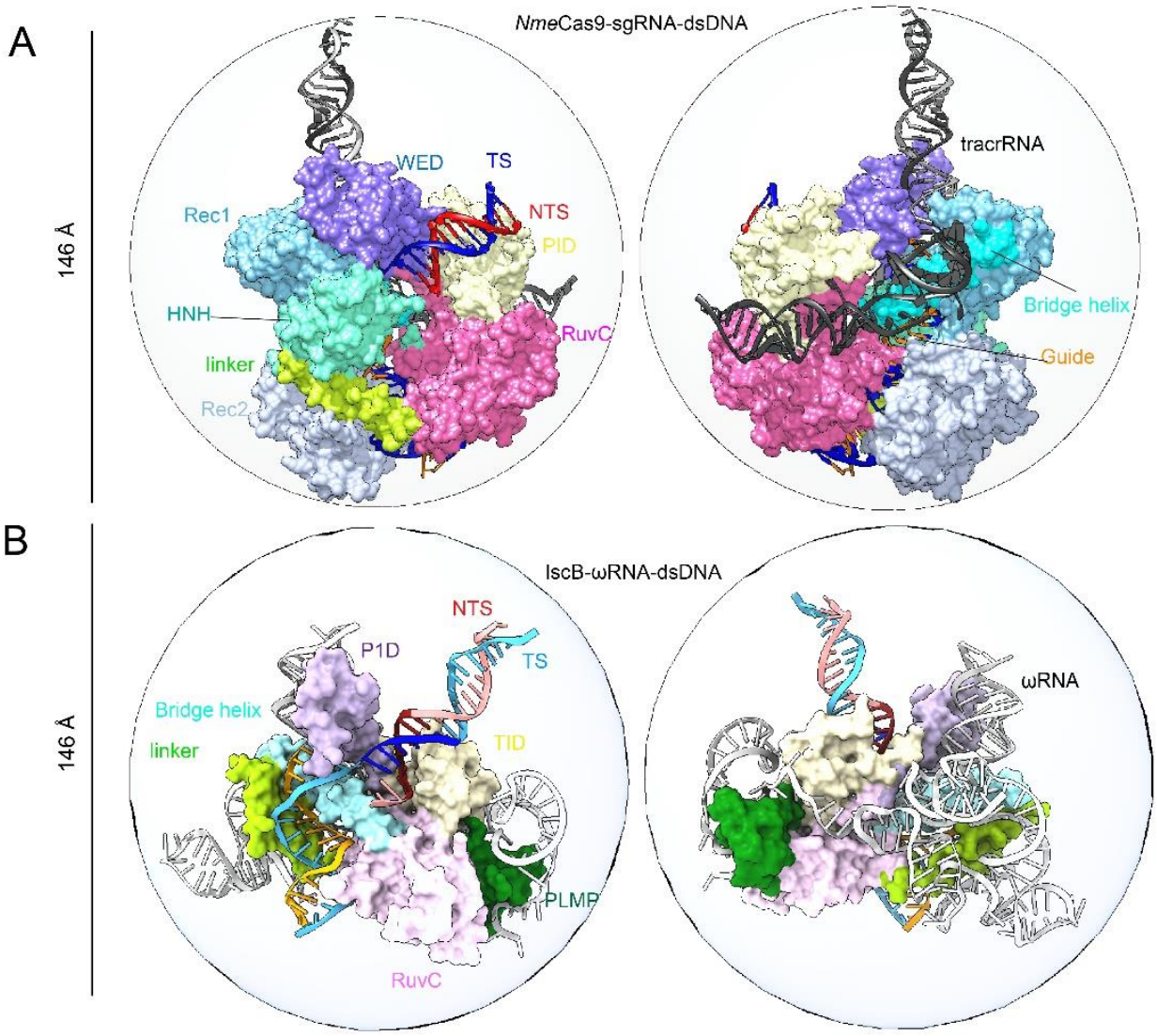

Fig. S4. Structural comparison between NmeCas9 RNP and IscB-ωRNA. The NmeCas9 RNP (PDB:6JDV) is significantly bigger in dimension, fuller in the Z dimension, and makes more extensive contacts with the DNA/RNA heteroduplex in the R-loop region. The lower portion of the R-loop is better protected by the Cas9 RNP, in particular.

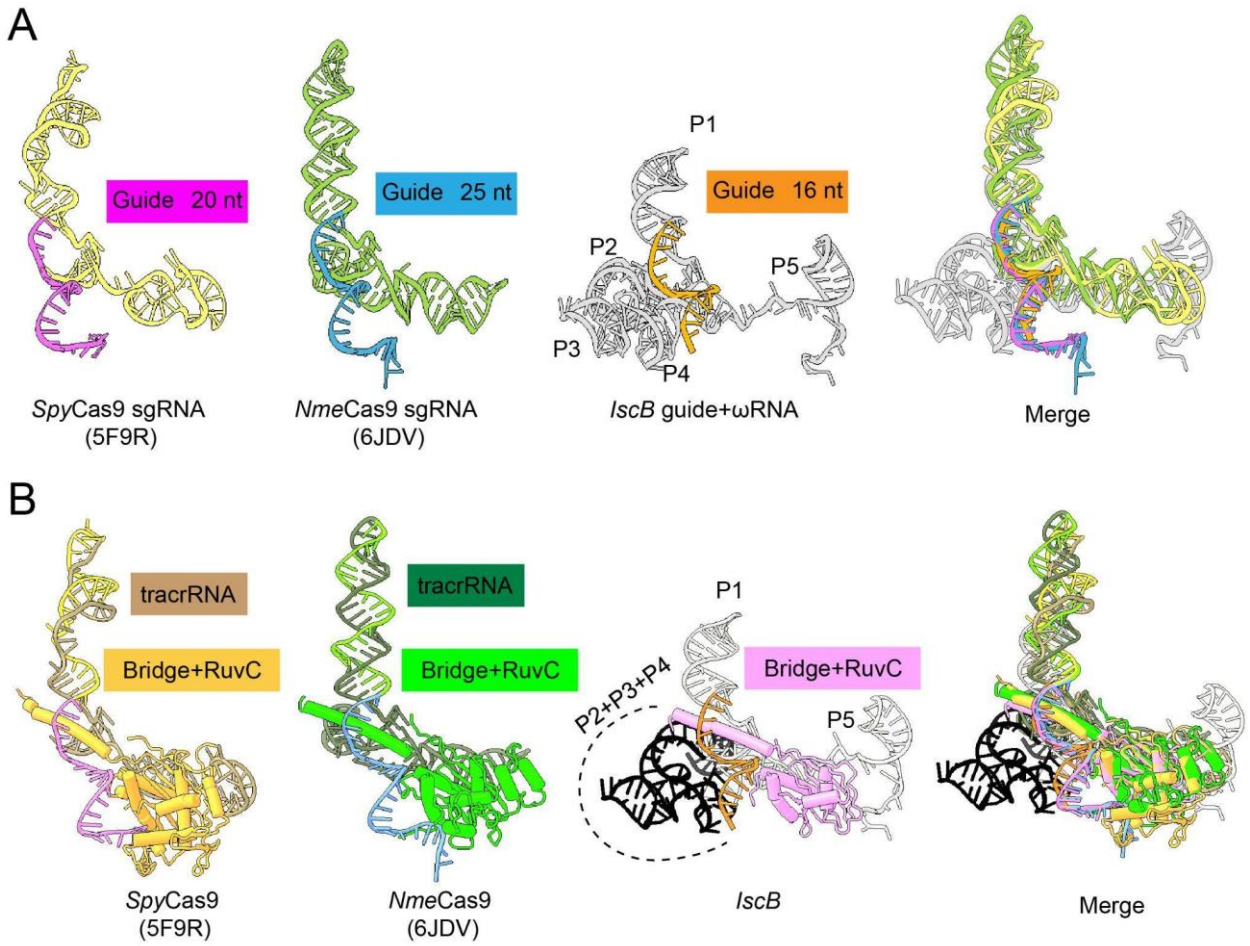

Fig. S5. Comparative structural analysis of ωRNA and core IscB domains with tracrRNA, guide RNA, and core Cas9 domains

(A) Structural comparison between the RNA components of the SpyCas9, NmeCas9, and IscB RNP. All three elements aligned showing structural conservation of ωRNA elements in Cas9 crRNA and tracrRNA. **(B)** Structural comparison between core protein domains and RNA components of SpyCas9, NmeCas9, and IscB. The bridge helix and RuvC domain are conserved across SpyCas9, NmeCas9, and IscB. All three elements aligned showing structural conservation of the bridge helix, RuvC domains, and ωRNA elements in Cas9 crRNA and tracrRNA.

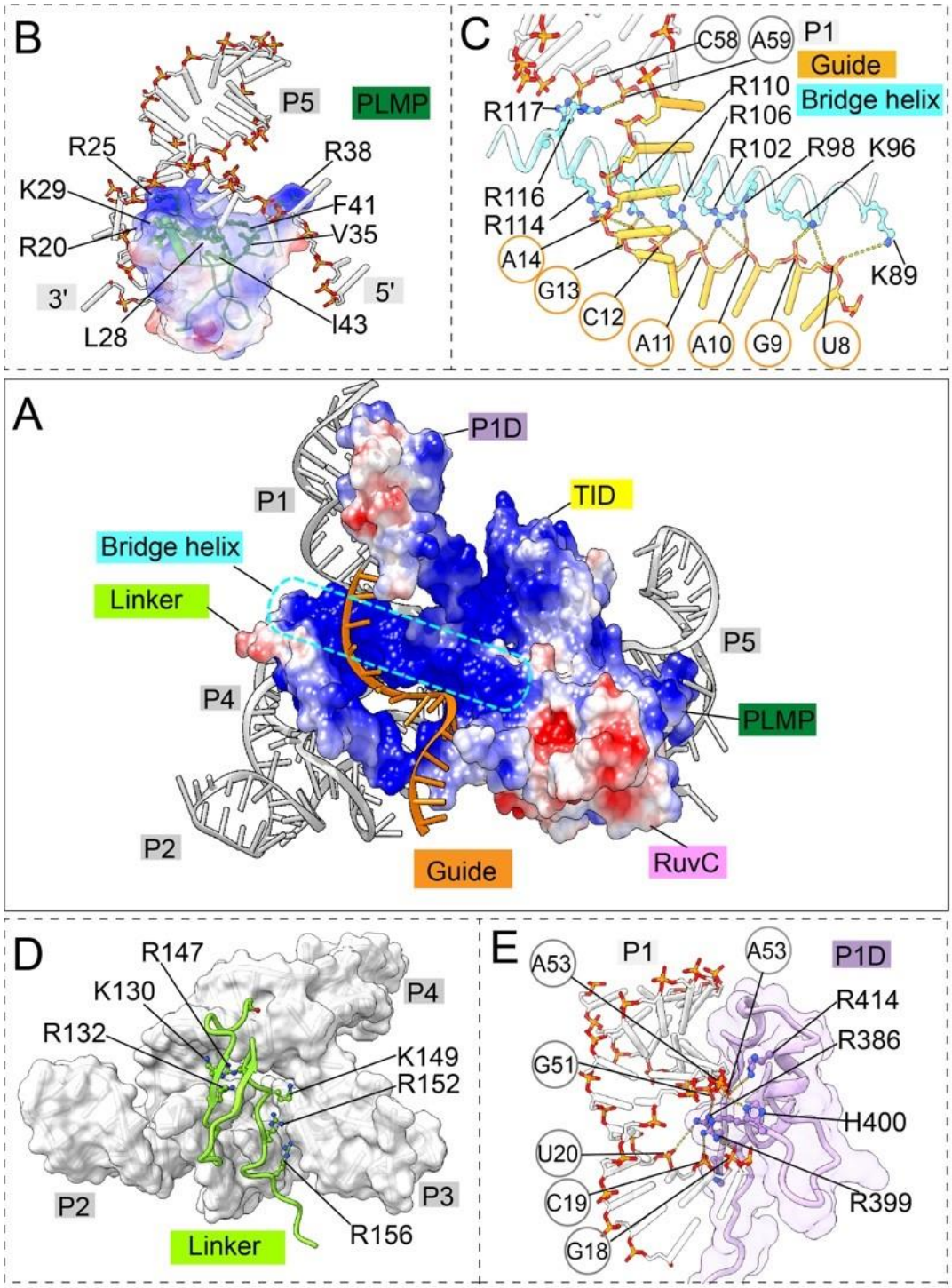

Fig. S6. IscB protein domain interactions with ωRNA and guide RNA.
(A) Electrostatic surface representation of IscB superimposed with the cartoon representation of ωRNA. IscB displays extensive positive charges (in blue) on surface for nucleic acid interaction. The bridge helix is boxed in light blue. **(B)** Close-up view of the IscB PLMP domain interactions with the base of P5 in ωRNA. **(C)** Close-up view of the bridge helix domain making consecutive phosphate backbone contacts to the guide RNA. **(D)** Close-up view of the IscB β-hairpin+linker domain to the P3 and J2 helices in the ωRNA lobe. **(E)** Close-up view of P1 interaction domain (P1D) contacting P1 of ωRNA.

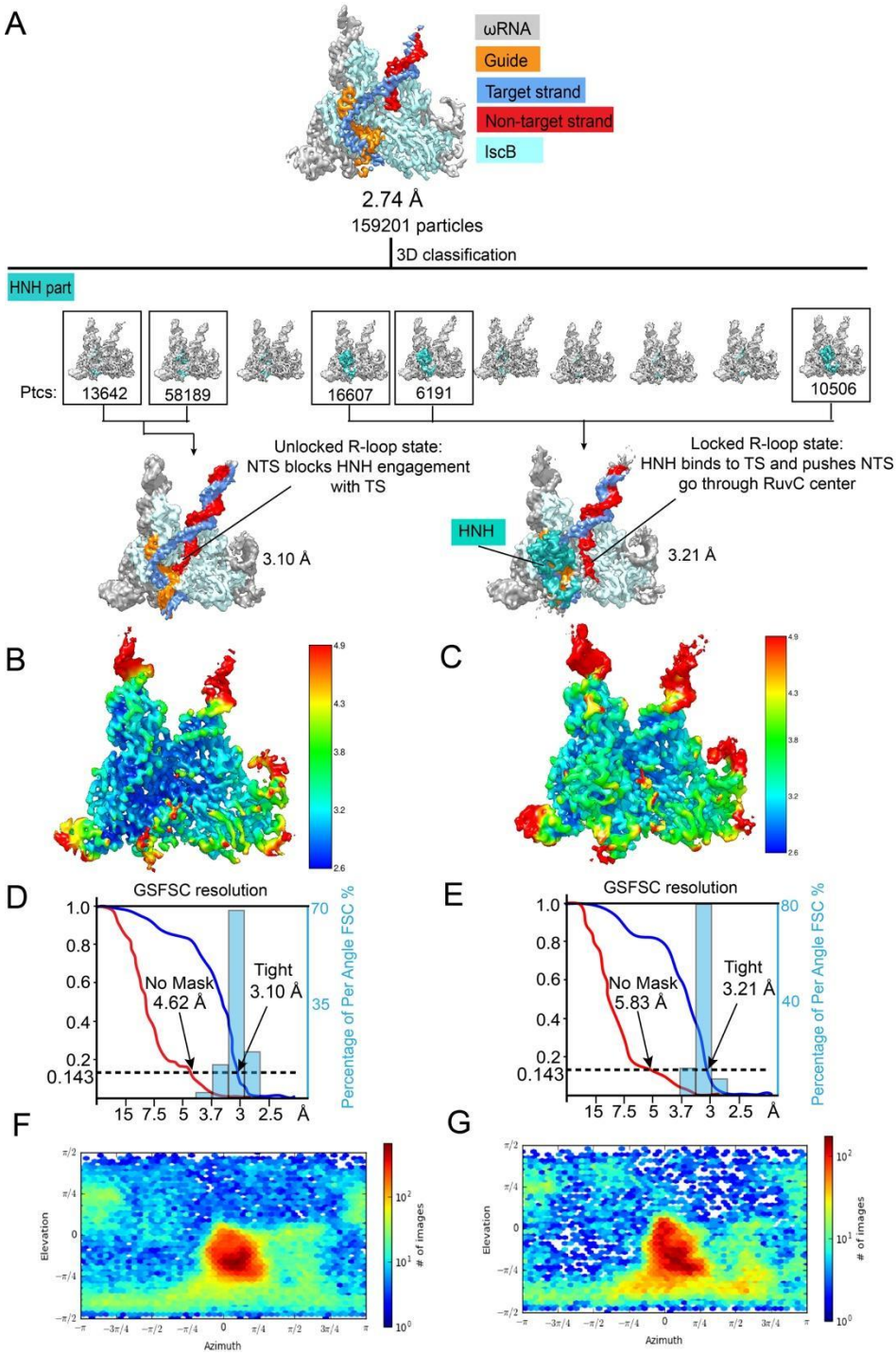

Fig. S7. Post-refinement to resolve HNH-docked conformational state. (**A**) Workflow to post-refine the high-resolution IscB-ωRNA/DNA data set. Finer 3D classification to partition HNH-docked conformational state (locked R-loop, 3.1 Å resolution) from the undocked state (unlocked R-loop, 3.2 Å resolution). Out of the 160,000 particles, ~40,000 exist in the HNH-docked state. (**B**, **C**) Local resolution distribution and (**D**, **E**) Fourier Shell Correlations of the unlocked and locked R-loop state, respectively. The gold-standard cutoff (FSC = 0.143) is marked with a dotted line. (**F**, **G**) Direction distribution plot of the unlocked and locked R-loop state, respectively.

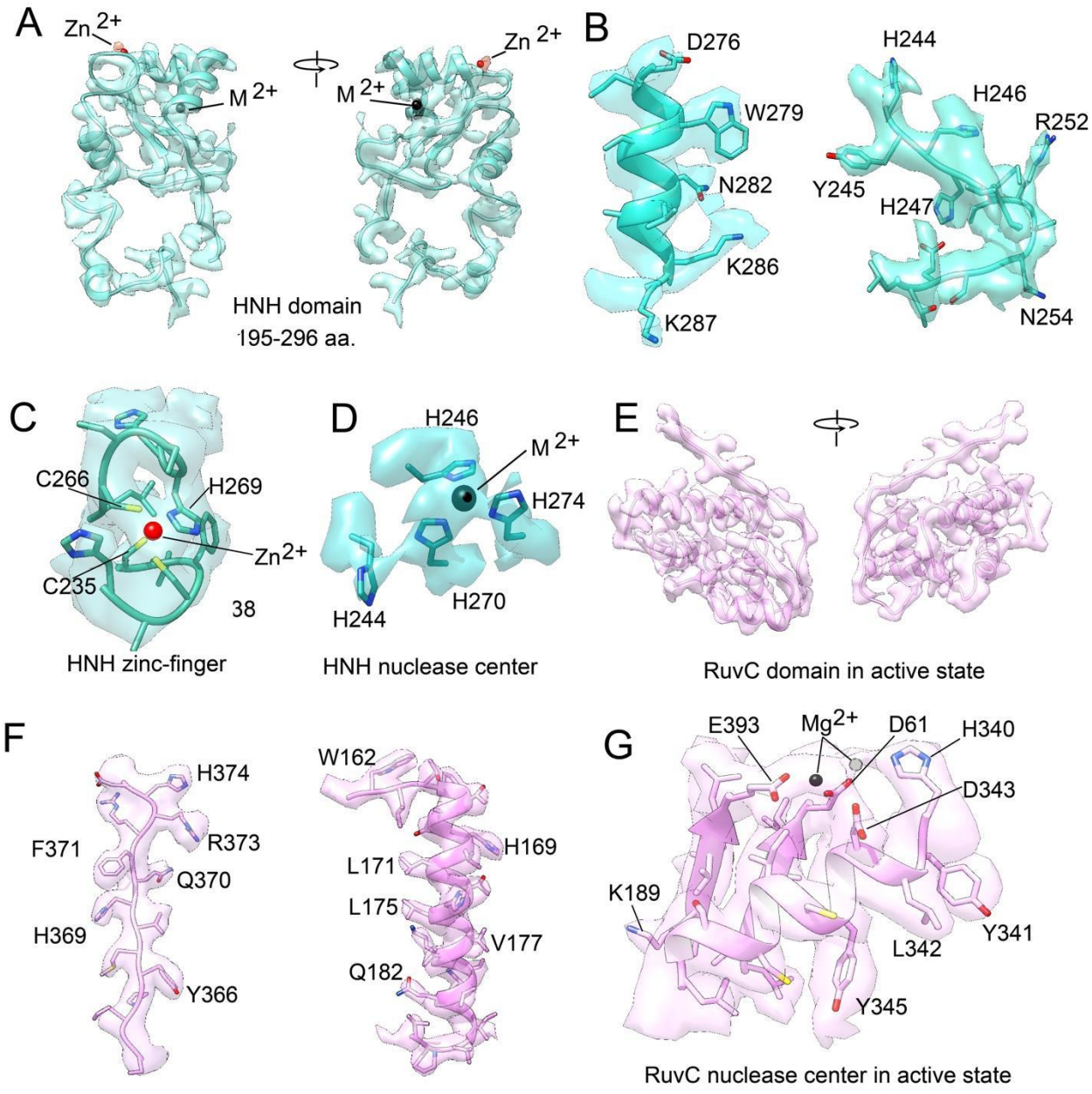

Fig. S8. Local density for HNH and RuvC domains in locked R-loop (active) state. (**A**) EM density for HNH domain in locked R-loop state. (**B**) EM local densities for representative regions in the HNH domain. (**C**) EM local density of zinc finger in HNH domain. (**D**) EM local density of HNH active site showing metal ion in black. (**E**) EM density for RuvC domain in locked R-loop state. (**F**) EM local densities for representative regions in the RuvC domain. (**G**) Local EM density of the RuvC active site showing metal ions. Metal ion in black seen in EM density. Metal ion in gray is expected but not seen in density due to phosphorothioate substitution in NTS-DNA.

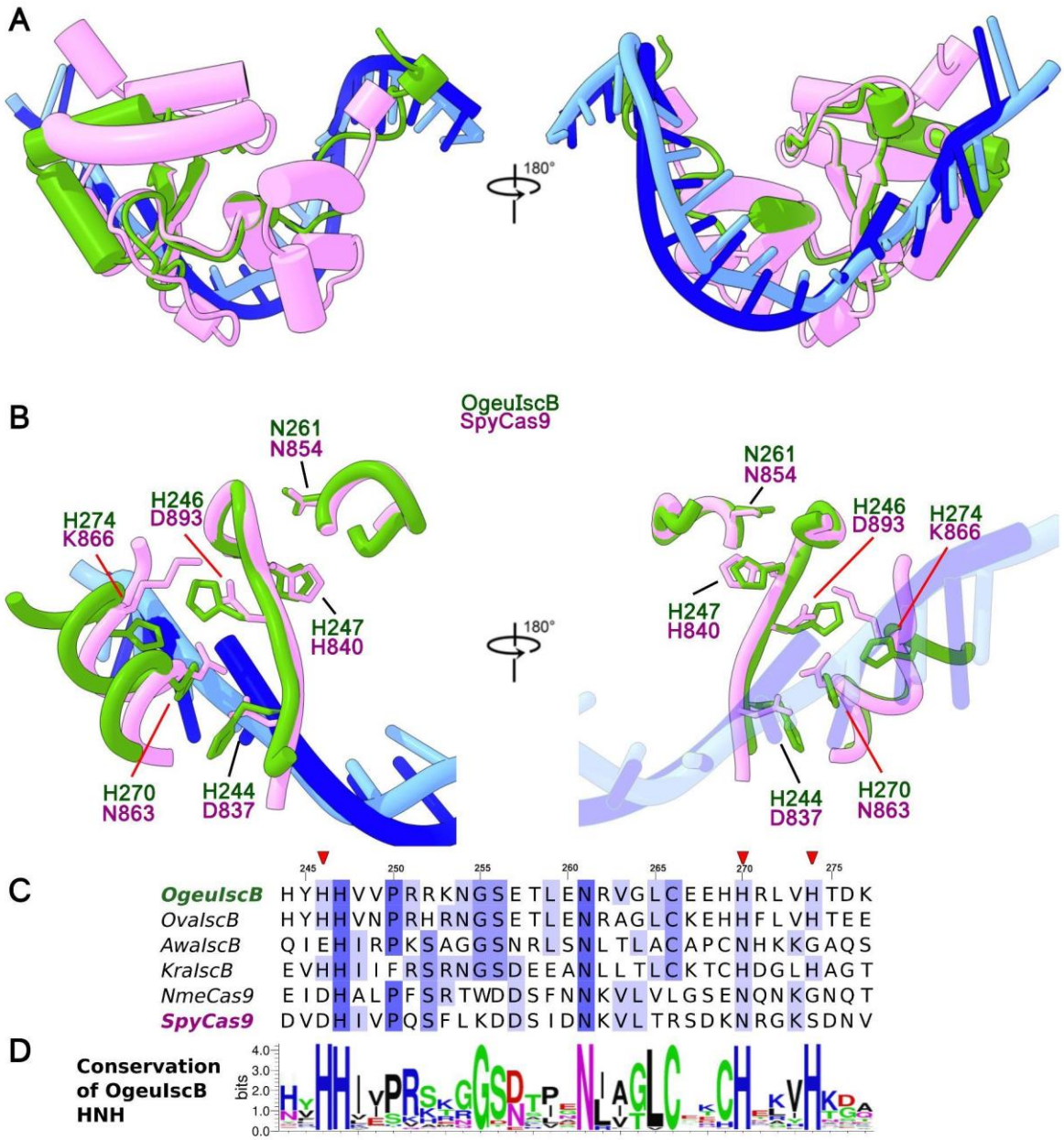

Fig. S9. Comparison of IscB and Cas9 HNH active site. (**A**) Structural alignment of HNH doman and TS-DNA of SpyCas9 (PDB: 7S4X) and IscB. OgeuIscB, green; OgeuIscB TS-DNA, light blue; SpyCas9, pink; SpyCas9 TS-DNA, blue. (**B**) Close-up structural alignment of the HNH active site of SpyCas9 and IscB RNP. (**C**) Amino acid sequence alignment of HNH active site. Red triangles mark the Histidine residues coordinating a metal ion in the OgeuIscB structure. Sequence is numbered according to OgeuIscB amino acid sequence. (**D**) Weblogo of HNH active site of OgeuIscB aligned with top 99 blastp hits in NCBI NR database.

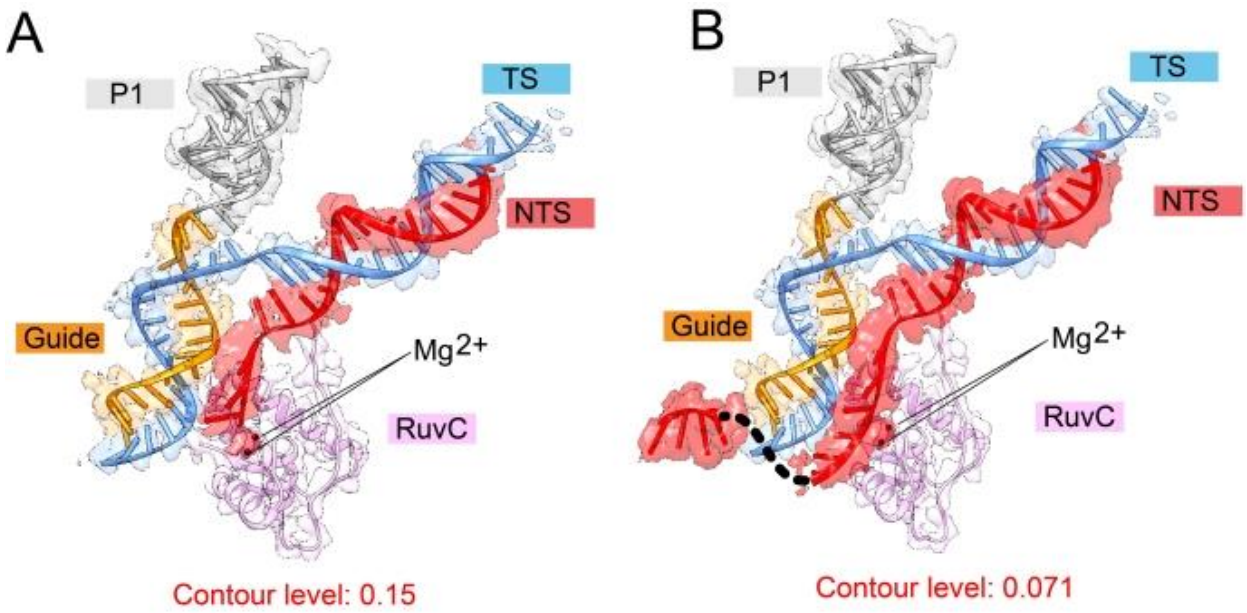

Fig. S10. NTS-DNA in RuvC nuclease center. (**A**) EM local density of NTS-DNA in locked R-loop (active) structure. NTS-DNA is not seen exiting the nuclease center at high contour level (0.15). (**B**) EM local density of NTS-DNA in locked R-loop (active) structure at higher contour level (0.071) showing that phosphorothioate bonds in NTS-DNA strand are intact in cryo-EM sample. NTS-DNA is seen exiting nuclease center. NTS-DNA strand in TAM distal R-loop is not observed due to high flexibility.

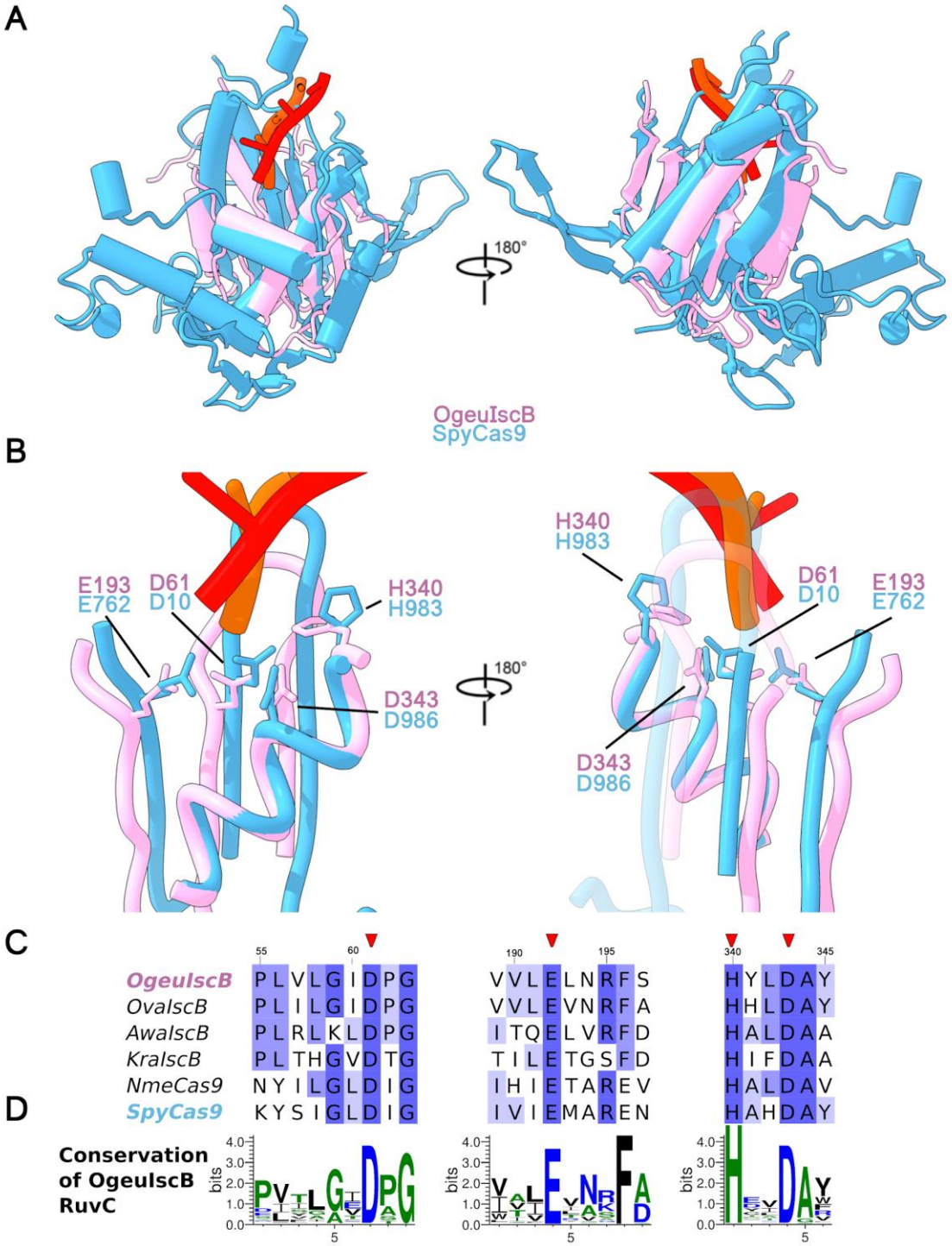

Fig. S11. Comparison of IscB and Cas9 RuvC active site. (**A**) Structural alignment of the RuvC domain and NTS-DNA of SpyCas9 (PDB: 7S4X) and IscB. OgeuIscB, pink; OgeuIscB NTS-DNA, orange; SpyCas9, light blue; SpyCas9 NTS-DNA, red. (**B**) Close-up of RuvC active site of SpyCas9 (PDB: 7S4X) and IscB RNP. (**C**) Amino acid sequence alignment of RuvC active site. Red triangles mark the active site residues. Sequence is numbered according to OgeuIscB amino acid sequence. (**D**) Weblogo of RuvC active site of OgeuIscB aligned with top 99 blastp hits in NCBI NR database.

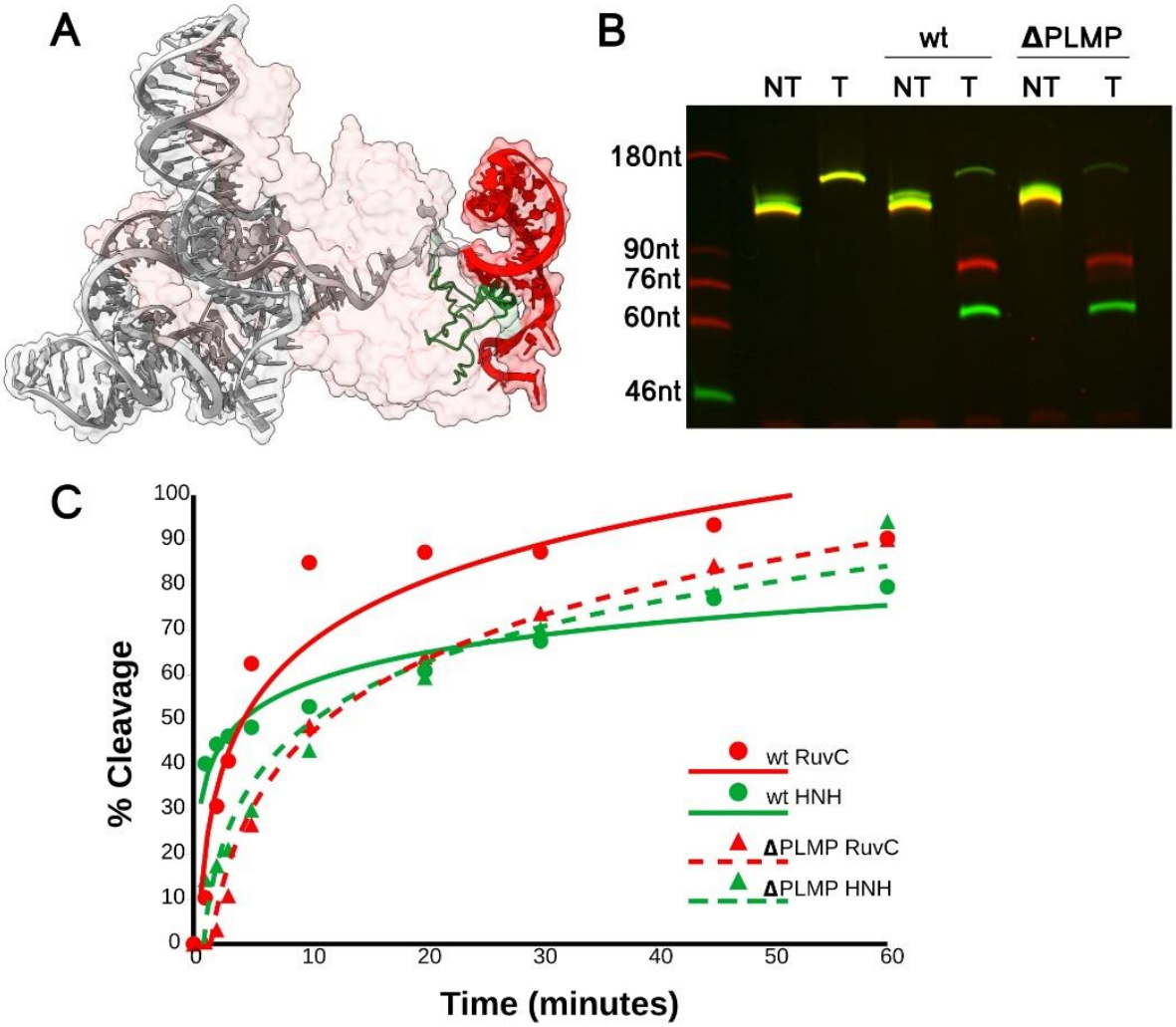

Fig. S12. PLMP mutant cleavage. (**A**) Cyro-EM reconstruction of IscB highlighting PLMP domain (green) and P5 (red). (**B**) Denaturing urea-PAGE cleavage gel showing RNA guided DNA cleavage with IscB ΔPLMP. T (target dsDNA), NT (non-target dsDNA control). (**C**) Time resolved cleavage of wt IscB compared with ΔPLMP IscB.

Table S1. Cryo-EM data collection, refinement, and validation statistics

Name PDB ID EMDB ID	IscB-ωRNA/Target (7UTN) (EMD-26782)	Unlocked R-loop state (8CSZ) (EMD-26994)	Locked R-loop state (8CTL) (EMD-26976)
Data collection and Processing (for each dataset)			
Microscope	Krios G3i	Krios G3i	Krios G3i
Voltage (keV)	300	300	300
Camera	K3	K3	K3
Magnification	81,000	81,000	81,000
Pixel size at detector (Å/pixel)	1.07Å	1.07Å	1.07Å
Total electron exposure (e^{-}/Å^2)	50	50	50
Exposure rate (e-/pixel/sec)	15	15	15
Number of frames collected during exposure	50	50	50
Defocus range (μm)	0.8 – 2.5	0.8 – 2.5	0.8 – 2.5
Phase plate (if used)	No	No	No
- phase shift range (in degrees)			
- number of images per phase plate position			
Automation software (EPU, SerialEM or manual)	EPU	EPU	EPU
Tilt angle (if grid was tilted)	No	No	No
Energy filter slit width (if used)	No	No	No
Micrographs collected (no.)	3956	3956	3956
Micrographs used (no.)	3956	3956	3956
Total extracted particles (no.)	4,076,994	4,076,994	4,076,994
For each reconstruction:			
Refined particles (no.)	4,076,994	4,076,994	4,076,994
Final particles (no.)	159,201	71,831	33,304
Point-group or helical symmetry parameters	C1	C1	C1
Estimated error of translations/rotations (if available)	N/A	N/A	N/A
Resolution (global, Å)	2.7	3.1	3.2
FSC 0.5 (unmasked/masked)	2.0 – 10	2.5 – 10	2.5 – 10
FSC 0.143 (unmasked/masked)	N/A	N/A	N/A
Resolution range (local, Å)	-78	-78	-78
Resolution range due to anisotropy (Å)	Global	Global	Global
Map sharpening *B* factor (Å^2) / (B factor Range)			
Map sharpening methods			
Model composition (for each model)			
Protein	397	401	494
Ligands	0	0	3
RNA/DNA	228	233	236
Model Refinement (for each model)			
Refinement package	CryoSPARC	CryoSPARC	CryoSPARC
- real or reciprocal space	Real	Real	Real
- resolution cutoff	2.78	3.10	3.20
Model-Map scores			
-CC	N/A	N/A	N/A
- Average FSC	N/A	N/A	N/A
B factors (Å^2)	76.1	82.4	86.0
Protein residues	65.9	68.3	72.3
Ligands	N/A	N/A	N/A
RNA/DNA	81.9	85.4	96.7

R.m.s. deviations from ideal values			
Bond lengths (Å)	0.007	0.009	0.005
Bond angles (°)	0.674	0.798	0.644
Validation (for each model)			
MolProbity score	1.67	3.24	1.75
CaBLAM outliers	N/A	N/A	N/A
Clashscore	8.15	31.1	11.2
Poor rotamers (%)	0.00	0.00	0.00
C-beta deviations	0.00	0.06	0.00
EMRinger score (if better than 4 Å resolution)	N/A	N/A	N/A
Ramachandran plot			
Favored (%)	98.22	92.41	95.17
Outliers (%)	0.00	0.00	0.00

Movie S1. Rotating views of the IscB-ωRNA/DNA cryo-EM reconstruction.

Movie S2. Rotating views and alignment of IscB-ωRNA-dsDNA and SpyCas9-sgRNA-dsDNA complex.

Movie S3. Rotating views and superposition of ωRNA and sgRNA of SpyCas9. RNA regions are labeled in the movie.

Movie S4. Structural basis of TAM recognition in IscB.

Movie S5. Rotating views and comparison of unlocked and locked R-loop states of IscB-ωRNA-dsDNA.

Movie S6. Structural basis of cleavage mechanism in HNH and RuvC domains. In the unlocked R-loop state, HNH blocks NTS-DNA for entering the RuvC cleavage site, HNH also cannot contact TS-DNA. As the result, no DNA cleavage takes place. In locked R-loop state, the HNH domain passes underneath NTS-DNA, binds the RNA/TS-DNA heteroduplex, and is catalytically competent to cleave the TS-DNA. The NTS-DNA in turn is allowed to enter the RuvC center for cleavage. The two events take place in an ordered fashion, which explains why TS-DNA cleavage is faster than the NTS-DNA cleavage. In essence, HNH allosterically controls the cleavage activity of RuvC in IscB. A similar mechanism is expected to take place in Cas9.